Burns & Trauma, 2022, 10, tkac001
https://doi.org/10.1093/burnst/tkac001
Research Article

OXFORD

Research Article

Curcumin-incorporated 3D bioprinting gelatin methacryloyl hydrogel reduces reactive oxygen species-induced adipose-derived stem cell apoptosis and improves implanting survival in diabetic wounds

Sizhan Xia[1,†*], Tingting Weng[1,†], Ronghua Jin[1], Min Yang[1], Meirong Yu[2], Wei Zhang[1], Xingang Wang[1,*] and Chunmao Han[1,*]

[1]Department of Burns and Wound Care Center, Second Affiliated Hospital of Zhejiang University College of Medicine, Hangzhou 310000, China and [2]Clinical Research Center, The Second Affiliated Hospital of Zhejiang University College of Medicine, Hangzhou 310000, China

*Correspondence. Xingang Wang, E-mail: wangxingang8157@zju.edu.cn; Chunmao Han, zrssk@zju.edu.cn
[†]These authors contributed equally to this work.

Received 6 August 2021; Revised 7 December 2021; Accepted 3 January 2022

Abstract

Background: Gelatin methacryloyl (GelMA) hydrogels loaded with stem cells have proved to be an effective clinical treatment for wound healing. Advanced glycation end product (AGE), interacting with its particular receptor (AGER), gives rise to reactive oxygen species (ROS) and apoptosis. Curcumin (Cur) has excellent antioxidant activity and regulates intracellular ROS production and apoptosis. In this study, we developed a Cur-incorporated 3D-printed GelMA to insert into adipose-derived stem cells (ADSCs) and applied it to diabetic wounds.
Methods: GelMA hydrogels with Cur were fabricated and their *in vitro* effects on ADSCs were investigated. We used structural characterization, western blot, ROS and apoptosis assay to evaluate the antioxidant and anti-apoptotic activity, and assessed the wound healing effects to investigate the mechanism underlying regulation of apoptosis by Cur via the AGE/AGER/nuclear factor-κB (NF-κB) p65 pathway.
Results: A 10% GelMA scaffold exhibited appropriate mechanical properties and biocompatibility for ADSCs. The circular mesh structure demonstrated printability of 10% GelMA and Cur-GelMA bioinks. The incorporation of Cur into the 10% GelMA hydrogel showed an inhibitory effect on AGEs/AGER/NF-κB p65-induced ROS generation and ADSC apoptosis. Furthermore, Cur-GelMA scaffold promoted cell survival and expedited *in vivo* diabetic wound healing.
Conclusions: The incorporation of Cur improved the antioxidant activity of 3D-printed GelMA hydrogel and mitigated AGE/AGER/p65 axis-induced ROS and apoptosis in ADSCs. The effects of scaffolds on wound healing suggested that Cur/GelMA-ADSC hydrogel could be an effective biological material for accelerating wound healing.

Key words: Curcumin, 3D printing, GelMA, Advanced glycation end products, Adipose-derived stem cells, Wound healing

© The Author(s) 2022. Published by Oxford University Press.
This is an Open Access article distributed under the terms of the Creative Commons Attribution-NonCommercial License (http://creativecommons.org/licenses/by-nc/4.0/), which permits non-commercial re-use, distribution, and reproduction in any medium, provided the original work is properly cited. For commercial re-use, please contact journals.permissions@oup.com

Downloaded from academic.oup.com/burnstrauma/article/doi/10.1093/burnst/tkac001/6547993 by guest on 14 October 2026

Highlights

- This study is the first to examine that 3D printed curcumin-GelMA scaffold alleviates ROS generation and apoptosis in ADSCs treated with AGEs.
- This study is the first to show that curcumin is involved in the inhibitory effect of AGEs/AGER-induced NF-κB transportation to the nucleus and caspase-3 activation in ADSCs.
- This study is the first to discuss that ADSCs encapsulated into 3D printing curcumin-GelMA can expedite diabetic wound healing *in vivo*.

Background

Chronic wounds caused by diabetes often result in repeated hospitalization, reduced quality of life and, in severe cases the involvement of organs and limbs, often requiring amputation [1–3]. Current treatments for diabetic wounds are not completely effective. Therefore, there is an urgent need for novel treatments to prevent and treat chronic diabetic wounds. Many previous studies reported that tissue engineering technology can be used for wound healing and mesenchymal stem cells (MSCs) are the ideal seed cells [4, 5]. Originally derived from mesoblasts, adipose tissue-derived stem cells (ADSCs) can easily be obtained using minimally invasive techniques; they have the capacity for multidirectional differentiation and possess considerable self-renewal ability. In addition, they have been shown to accelerate wound healing [6]. Damaged skin has a harsh microenvironment with increased reactive oxygen species (ROS) and inflammation, leading to decreased vitality and increased apoptosis, which impede wound healing [7, 8]. Therefore, it is essential to improve seed cell vitality for wound healing; determining the mechanisms underlying seed cell vitality may lead to novel approaches to wound healing.

Advanced glycation end products (AGEs) are stable products of complex reactions, including condensation, rearrangement, lysis and oxidative modification, which are considerably increased in diabetes mellitus [9]. AGEs in diabetes can cause much pathological damage, including skin fibroblast and vascular endothelial cell apoptosis, which impedes wound healing [10, 11]. AGEs cause pathological changes by stimulating signal transduction pathways through binding to specific advanced glycation end product receptors (AGERs) on the cell membrane [12]. AGERs consist of extracellular domains, a single transmembrane spanning helix and a cytoplasmic domain, which are essential for signal transduction [13]. Previous studies have proposed that the binding of AGEs to AGERs promotes ROS and inflammatory responses, which causes endothelial dysfunction and activates transcription factor nuclear factor-κB (NF-κB) [14, 15]. AGE/AGER interaction activates various signaling pathways, including those related to apoptosis.

Curcumin (Cur) is a polyphenolic substance extracted from the rhizomes of curcumae with strong antioxidant, anti-inflammatory, anti-bacterial and anti-hyperblastosis activities due to its role in pleiotropic signaling transmission [16–18]. Numerous studies have reported the efficacy of Cur treatment for chronic wounds and diabetes. Although Cur has a wide range of activities, its physical and chemical properties (poor water solubility, chemical instability and rapid degradation) limit its medicinal use. Previous studies have reported that gelatine methacryloyl (GelMA) can be used to deliver drugs with desirable release profiles [19]. The incorporation of methacrylate groups in gelatine is responsible for the tunable mechanical properties, biocompatibility and favorable drug release properties of GelMA, by affecting the degree of crosslinking by ultraviolet light [20, 21]. These properties make GelMA the ideal bioink for 3D bioprinting. In this research, we used Cur, an antioxidant and anti-apoptosis element, to regulate the unfavorable microenvironment of the diabetic wound, which is detrimental to the survival of ADSCs. Therefore, Cur was loaded into 3D bioprinting GelMA hydrogels to provide an appropriate microenvironment for ADSCs. Then, we evaluated the role of Cur in ADSCs with AGEs, and demonstrated that Cur modulated the effects of ADSCs on diabetic wounds by targeting the AGE/AGER/p65 pathway.

Methods

The material

GelMA synthesis Briefly, 1 g of gelatin was dissolved in PBS at 10% mass fraction and 1 mL of methacrylic anhydride (J&K Scientific, Beijing, China) was slowly added and reacted in a waterbath at 60°C for 2 h, during which the temperature was kept constant. After the reaction was completed, the solution was filtered and dialyzed in a dialysis bag (3.5 kDa; Beyotime, Shanghai, China) for 3 d and then lyophilized (NO.7670030; Labconco, Kansas, MO, USA). Lyophilized GelMA was dissolved in PBS containing 0.3% lithium 2,4,6-trimethylbenzoyl phosphate (Tokyo Chemical Industry; Tokyo, Japan) as a photoinitiator at 50°C [22].

3D bioprinting of the GelMA scaffold 3D GelMA scaffolds were fabricated using an extruded bioprinter (BioArchitect Pro; Regenovo, Hangzhou, China). The temperature of the nozzle and platform was kept at ~20 and 18°C, respectively, and the printing speed and pressure were set at 5 mm/s and 0.2 MPa, respectively. The GelMA and the cell suspension containing Cur were blended thoroughly to obtain 10% GelMA, 20 μM Cur and 5×10^5 cells/mL of ADSCs. The bioink was printed as a circular mesh structure under a 210 μm diameter nozzle, cross-linked with blue light for 20–30 s and then placed in DMEM/F12 containing 10% fetal bovine serum (FBS; Invitrogen Life Technologies) for incubation.

Downloaded from academic.oup.com/burnstrauma/article/doi/10.1093/burnst/tkac001/6547993 by guest on 14 October 2026

Isolation and culture of human ADSCs ADSCs were obtained from liposuction patients aged 30–45 years. All donors signed informed consent at the Second Affiliated Hospital of Zhejiang University College of Medicine. Adipose tissue was digested with 0.1% collagenase I (Invitrogen, Carlsbad, CA, USA) for 45–60 min at 37°C, then centrifuged and filtered to obtain ADSCs and cultured in DMEM/F12 with 10% FBS.

Preparation of cur-GelMA hydrogel A 0.368 mg portion of curcumin (Beyotime, Shanghai, China) was dissolved in 1 mL of DMSO to form a 1 mM solution and stored at −20°C until use. Cur was added to the GelMA hydrogel and mixed evenly to achieve the required concentration (20 μM) of the Cur-GelMA solution.

Scanning electron microscopy After lyophilization of 10% GelMA and 10% Cur-GelMA hydrogel for 24–48 h, samples were coated with gold–palladium using an E-1010 ion sputterer (High-Tech Group, Tokyo, Japan) for 4–5 min and analyzed by XL30 scanning electron microscope (SEM) (Philips, Eindhoven, The Netherlands) and SU-8010 SEM (SEM; Hitachi).

Porosity The hydrogel pores were calculated directly using ImageJ. Porosity = pore area/total area.

Swelling ratio GelMA hydrogels were immersed in PBS at 37°C for 24 h, weighed and recorded as Wwet, then dried by lyophilization for 24 h, weighed and recorded as Wdry. Swelling ratio (SR) = (Wwet − Wdry)/Wdry × 100% [22].

Atomic force microscopy A Park XE-70 atomic force microscope (AFM) (Park Systems Inc., Suwon, South Korea) was used to analyze single molecule force spectroscopy of GelMA. The samples were placed on the carrier table of the AFM and observed at room temperature and under atmospheric conditions. The probes used were commercially available silicon nitride (OMCL-TR400PSA; Olympus, Co. Ltd, Tokyo, Japan) with a force constant of $\backsim$0.08 N/m, a microcantilever length of 200 μm and an average spring constant of $\backsim 87.24 \pm 1.56$ pN/nm. The images were obtained in tap mode. The force distance curves were analyzed with Origin software.

Degradation The degradation of Cur was indirectly measured by the absorbance value. Cur was added to 2 mL of DMEM/F12 with 10% FBS to form a 20 μM solution. Samples were incubated at 37°C and 5% CO_2. After incubation, 200 μl of the solution was added to a 96-well plate and the absorbance value (420 nm) was measured using a microplate reader. DMEM/F12 medium containing 10% FBS without Cur served as a negative control.

Cell treatment According to a previous report, AGER expression did not increase with AGEs (800 μg/mL) in BMSCs for 24 h [23]. Studies have shown that Cur has cytotoxic effects at high concentrations (>25 μM) [24]. Therefore, AGEs (800 μg/mL, Biovision, Milpitas, CA, USA) and Cur (20 μM) were added to the ADSCs in Petri dishs or in GelMA scaffolds. A p65 inhibitor, pyrrolidinedithiocarbamate (PDTC) (30 μM; Beyotime), was also added to the cultured cells to block p-p65 activity.

Cell viability The live/dead assay was used to detect cell viability [live: calcein AM, dead: propidium iodide (PI); KeyGen Biotech Co., Ltd, Nanjing, China]. Samples were incubated in the solution (AM:PI:PBS = 1:1:1000) for 1 h at 37°C without light. The live/dead of ADSCs loaded in GelMA was directly detected using a fluorescence microscope without extracting ADSCs (calcein AM, excitation/emission: 488/525 nm; PI, excitation/emission: 488/690 nm).

Measurement of intracellular ROS ADSCs were incubated in the working solution (10 μM CM-H2DCFDA, Beyotime, Shanghai, China) for 1 h at 37°C in the dark. A fluorescence microscope and a flow cytometer (BD Biosciences, Franklin Lakes, NJ, USA) were used to detect intracellular ROS. The intracellular ROS of ADSCs loaded in GelMA was detected using a fluorescence microscope without extracting ADSCs (CM-H2DCFDA, excitation/emission: 488/525 nm) [25].

Apoptosis assay ADSC apoptosis was determined using V-FITC/PI according to the manufacturer's instructions (Beyotime). Flow cytometery was used to analyze the apoptosis rate. The apoptosis of ADSCs loaded in GelMA was directly detected using a fluorescence microscope without extracting ADSCs (Annexin V-FITC, excitation/emission: 488/525 nm; PI, excitation/emission: 488/690 nm).

Cell transfection The sequence for the AGER siRNA was as follows: AGER siRNA: 5′- GCCTCTGAACTCACAGCCA −3′ (GenePharma, Shanghai, China). ADSCs were cultured in 6-well plates for transfection using LipofectamineTM3000 (L3000150, Invitrogen, MC, USA) according to the manufacturer's instructions. After 48 h the transfected ADSCs were used for western blot, ROS and flow cytometry.

Western blot RIPA was applied to extract the total cellular protein, and a BCA protein assay kit was used to determine the protein concentration. The protein was transferred to a PVDF membrane and the primary antibody was incubated at 4°C overnight, followed by incubation with the secondary antibody (BA1054, Boster, Wuhan, China) at room temperature for 2 h. The primary antibodies were rabbit AGER (#55222, 1:500; Cell Signaling Technology/CST, Beverly, MA, USA), p65 (#3033, 1:500; CST), p-p65 (#8242, 1:500; CST) and β-actin (ab8227, 1:1000; Abcam, Cambridge, UK).

Caspase-3 activity assay Annexin V-mCherry and GreenNuc™ caspase-3 were used to detect caspase-3 activity (Beyotime). ADSCs were incubated in the solution (5 μL of annexin V-mCherry and 1 μL of GreenNuc™ caspase-3 substrate per 200 μL of binding buffer) for 30-45 min at 37°C without light. Cell membrane permeability Caspase-3

Downloaded from academic.oup.com/burnstrauma/article/doi/10.1093/burnst/tkac001/6547993 by guest on 14 October 2026

Substrate GreenNuc™ for the detection of caspase-3 activity in cultured cells can be used for real-time monitoring [26]. Immunofluorescence microscopy was used to obtain images (GreenNuc™, excitation/emission: 500/530 nm; Annexin V-mCherry, excitation/emission: 587/610 nm).

Cell immunofluorescence staining ADSCs were fixed with 4% paraformaldehyde for 30 min, followed by 0.2% Triton X-100 permeable cells for 1 h. ADSCs were incubated overnight at 4°C in the dark with the first antibody: p65 (1:200; CST) and p-p65 (1:200; CST). Subsequently, ADSCs were incubated with secondary antibody goat anti-rat IgG Alexa Fluor 488 (1:200; Boster, Wuhan, China) for 1 h at room temperature in the dark. DAPI (1:10000) was used for nuclear counterstaining (green, excitation/emission: 488/525 nm; red, excitation/emission: 594/610 nm).

***In vivo* ADSC survival assay** Cells were labeled with 1,1′-dioctadecyl-3,3,3′,3′-tetramethylindotricarbocyanine (DiR, US Everbright, Suzhou, China) prior to transplantation at 37°C for 30–45 min. Subsequently, 5×10^5 ADSCs were transplanted into the wound with or without 3D-printed 10% GelMA. At days 3, 7, 14 and 21 after transplantation, isoflurane anesthesia was administered to mice and an *in vivo* imaging system (IVIS) was used to trace ADSCs.

***In vivo* experiments** Thirty 6-week-old nu/nu athymic nude mice were used in this research (Experimental Animal Center of Zhejiang University). All animal experiments were conducted at the Animal Center of Zhejiang University and approved by Animal Care and Use Committee. Diabetes was induced in the mice by an intraperitoneal injection of 150 mg/kg of streptozocin (STZ) (Sangon Biotech Co., Ltd, Shanghai, China). Under ketamine anesthesia, a 15-mm punch was used to incise a full skin defect on the dorsal of nude mice and the wound edges were sutured with silicone rings to limit wound contraction due to skin contraction. The nude mice were implanted with 10% GelMA, 10% GelMA-ADSCs or 10% Cur-GelMA-ADSCs (20 μM Cur) scaffold immediately after surgery, with the GelMA scaffold acting as a negative control and the GelMA-ADSCs scaffold acting as a positive control. The surface of the wound was covered with Vaseline gauze and transparent film to maintain a moist environment and prevent external infection, and the dressing was changed every 2 days. The mice were sacrificed by administering an excessive dose of ketamine at 14 and 21 days after scaffold implantation; skin tissues were then subjected to further evaluation.

Histological analysis Samples were fixed in 4% paraformaldehyde for 24–48 h, dehydrated and paraffin-embedded and 5-6 μm paraffin sections were cut. Paraffin sections were heated at 60°C for 1 h, deparaffinized and rehydrated. The treated sections were subjected to subsequent experiments, including hematoxylin and eosin (H&E) staining, Sirius Red staining and TUNEL assay. The level of re-epithelialization was calculated as: (diameter of original wound−diameter of wound without epithelium)/(diameter of original wound) × 100% [27]. Total collagen and organized collagen were recorded by white light microscopy and polarized light microscopy, respectively, and their ratios were analyzed by ImageJ.

For immunohistochemical staining, the sections were incubated with rabbit AGEs (ab23722, 1:50; Abcam) overnight at 4°C; diaminobenzidine was used to produce a brown precipitate. The tissue sections were incubated for 60 min at room temperature with the secondary antibody. To evaluate the immunohistochemical staining, immunoreactivity was blindly assessed by two independent observers using light microscopy.

For immunofluorescence staining, the sections were incubated with rabbit CD-31 (ab281583, 1:500; Abcam) and mouse α smooth muscle actin (α-SMA; ab7817, 1:500; Abcam). Then, the tissue sections were incubated with secondary antibodies for 1 h at room temperature without light, including goat anti-rat IgG Alexa Fluor 488 and rat anti-mouse IgG Alexa Fluor 594 (1:200; Boster). DAPI (1:10000) was used for nuclear counterstaining. A fluorescent microscope was used to take photographs of the slides (green, excitation/emission: 488/525 nm; red, excitation/emission: 594/610 nm).

Statistical analysis

The data were processed using the statistical software SPSS 22.0 (IBM, Armonk, NY) and the measurement data obeyed the normal distribution and were expressed as means ± SD. A *t*-test was used for comparison between two groups at the same time point. One-way ANOVA was performed to compare the differences between multiple groups at the same point and two-way ANOVA for comparison between multiple groups at multiple time points. The statistical significance level was set at $p < 0.05$. In the figures, we used $*$ to denote *p*-values, in which $^{*}p < 0.05$, $^{**}p < 0.01$ and $^{***}p < 0.001$.

Results

Characterization of GelMA and Cur-GelMA scaffolds

The GelMA hydrogel and Cur were mixed to a final concentration of 10% GelMA [28, 29] and 20 μM Cur [30]. The SEM results showed that the Cur-GelMA and GelMA scaffolds had large internal pores and high porosity (Figure 1a–c). Importantly, the pore sizes of both scaffolds were suitable for cell proliferation (100–500 μm). Additionally, a SEM was used to characterize the scaffold morphology, which showed that Cur particles were uniformly adsorbed on GelMA (Figure 1d). The Cur-GelMA and GelMA scaffolds exhibited applicable SRs (Figure 1e), suggesting that both scaffolds maintained a moist wound and absorbed nutrients from tissue exudates [31]. Furthermore, we seeded ADSCs on a 10% GelMA scaffold to observe cell adhesion. The scaffold exhibited appropriate mechanical properties for developing

Downloaded from academic.oup.com/burnstrauma/article/doi/10.1093/burnst/tkac001/6547993 by guest on 14 October 2026

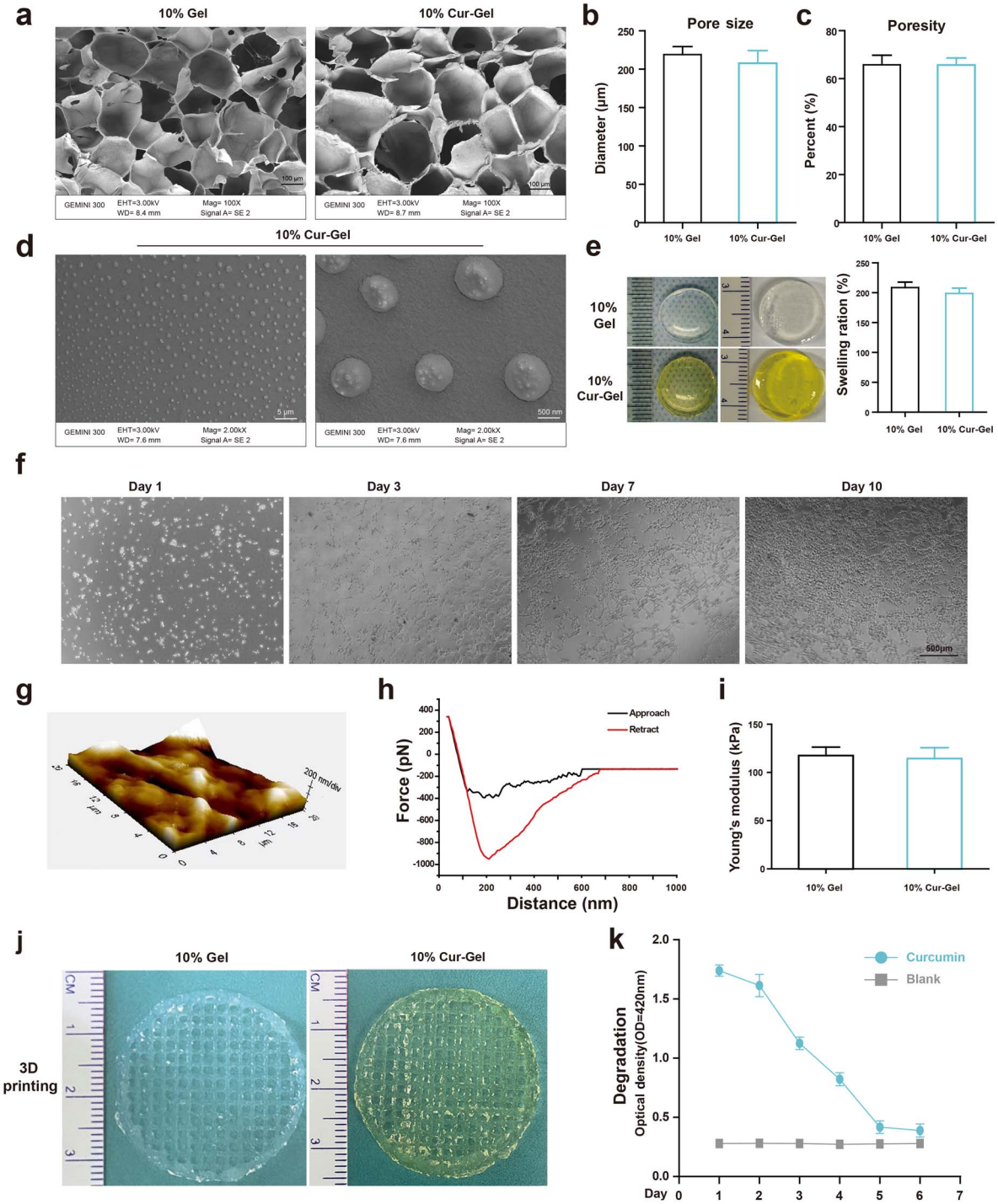

Figure 1. Structure of GelMA and Cur-GelMA scaffolds. (**a**) Scanning electron microscopy images of 10% GelMA and 10% Cur-GelMA. (**b, c**) Quantification of the pore size and porosity of GelMA and Cur-GelMA scaffolds. (**d**) Scanning electron microscopy images of Cur in GelMA scaffold showing smooth surface morphologies. The mean diameter of particles was 0.99 ± 0.12 μm. (**e**) Quantification of the swelling ratio of GelMA and Cur-GelMA scaffolds. (**f**) Representative images of ADSCs on 10% GelMA surfaces. (**g–i**) Typical atomic force microscopy curve and Young's modulus of GelMA. (**j**) Printability test of 10% GelMA and 10% Cur-GelMA hydrogels. (**k**) Cur degrades in DMEM/F12 with 10% FBS. *GelMA* Gelatin methacryloyl, *Cur* curcumin, *ADSC* adipose-derived stem cell

a confluent cluster of ADSCs on day 10 (Figure 1f). A typical atomic force microscopy curve and Young's modulus of GelMA hydrogels are shown in Figure 1g–i. The circular mesh structures (3 cm × 3 cm × 1 mm) were printed to demonstrate the printability of 10% GelMA and Cur-GelMA bioinks (Figure 1j). Cur degradation in culture medium (DMEM/F12 with 10% FBS) was evaluated for 6 days (Figure 1k).

Downloaded from academic.oup.com/burnstrauma/article/doi/10.1093/burnst/tkac001/6547993 by guest on 14 October 2026

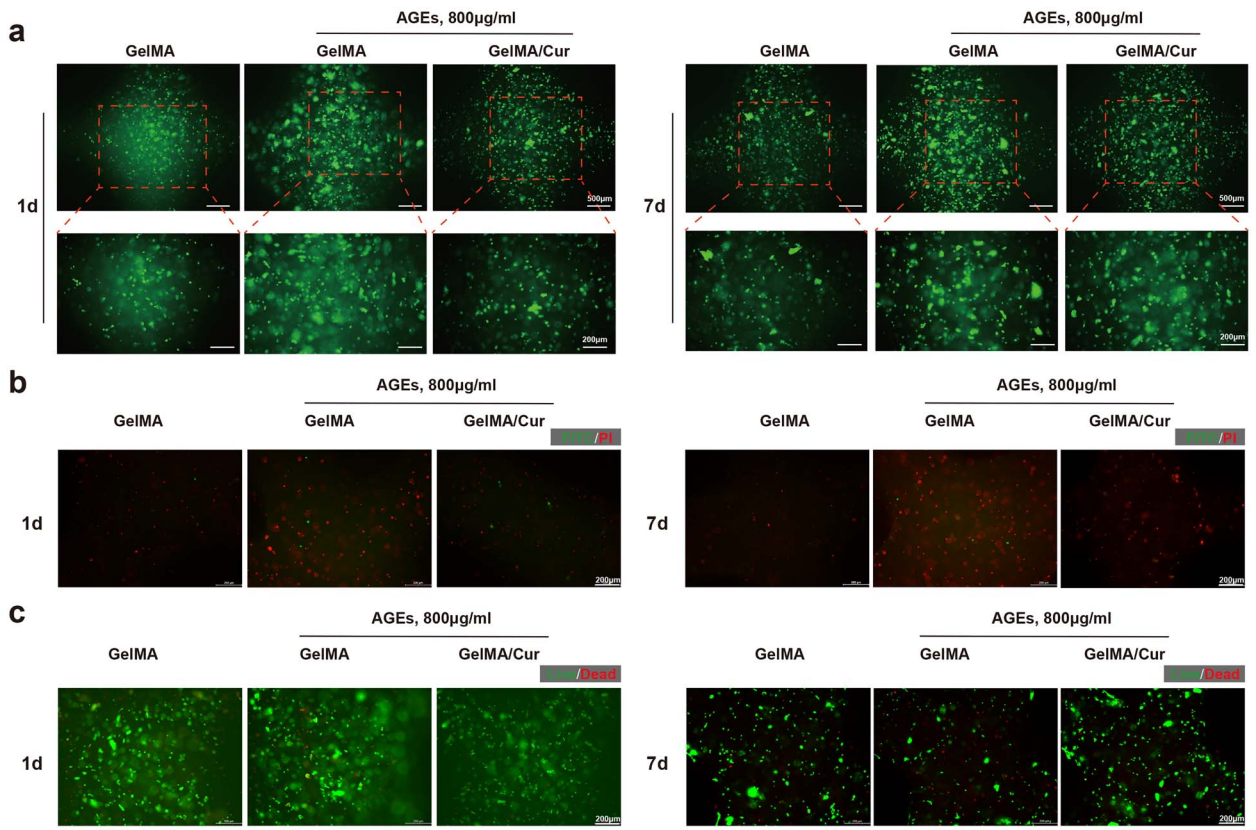

Figure 2. Effects of AGEs on ROS production, and the apoptosis and cell viability of ADSCs on 3D printing scaffolds. (**a**) Intracellular ROS levels were visualized with a fluorescence microscope. (**b**) ADSCs were stained with V-FITC/PI and visualized by fluorescence microscope. (**c**) Cell viability (live/dead fluorescence images) of ADSCs encapsulated in the 10% 3D printing GelMA scaffolds. *AGE* Advanced glycation end-product, *ROS* reactive oxygen species, *ADSC* adipose-derived stem cell, *GelMA* gelatin methacryloyl

Cur-GelMA scaffold alleviates ROS generation and apoptosis of ADSCs treated with AGEs

To detect whether Cur and AGEs affect ROS generation in ADSCs encapsulated into Cur-GelMA or GelMA scaffolds, samples were treated with or without AGEs (800 μg/mL). Fluorescence microscopy showed that ROS production was increased after AGEs incubation, but decreased in the Cur-incorporated GelMA scaffold on days 1 and 7 (Figure 2a). In addition, we further investigated whether AGEs and Cur were implicated in the modulation of ADSC apoptosis. FITC/PI staining indicated that AGEs increased cell apoptosis, which was attenuated by Cur by days 1 and 7 (Figure 2b). To investigate the biocompatibility of GelMA and Cur-GelMA scaffolds, we conducted a cell viability assay, which showed that Cur prevented AGE-induced cell death in the GelMA scaffold (Figure 2c). These data suggest that Cur encapsulated in the GelMA scaffold could inhibit AGE-induced ADSC ROS and apoptosis.

AGEs/AGER axis induces ROS production and apoptosis

To further investigate the interaction between AGEs/AGER, we examined the expression of AGER in ADSCs after transfection of siRNA and pretreatment with or without AGEs. The results showed that the levels of AGER were enhanced by AGE exposure, but significantly decreased after transfection with siAGER (Figure 3a). H2DCFDA probes were loaded onto ADSCs to detect intracellular ROS expression. Fluorescence microscopy and flow cytometry showed that AGEs treatment induced intracellular ROS production, but this was diminished after AGER knockdown (Figure 3b, c). Subsequently, according to flow cytometry, interfering with the expression of AGER attenuated AGEs-induced apoptosis (Figure 3d). These results suggested that the AGE/AGER axis increased ROS production and ADSC apoptosis.

Cur and NF-κB are implicated in ROS production and ADSC apoptosis

Cur can prevent intracellular ROS production and apoptosis of pancreatic beta cells [32]. Furthermore, the AGEs/AGER axis activates NF-κB, which leads to apoptosis [33]. To detect whether Cur affects AGER and p65 induced by AGEs, we detected AGER and p-p65 protein levels after AGEs pretreatment, with or without the NF-κB inhibitor PDTC. The results showed that AGER and p-p65 levels were decreased after Cur exposure, while the p-p65 level was significantly reduced after

Downloaded from academic.oup.com/burnstrauma/article/doi/10.1093/burnst/tkac001/6547993 by guest on 14 October 2026

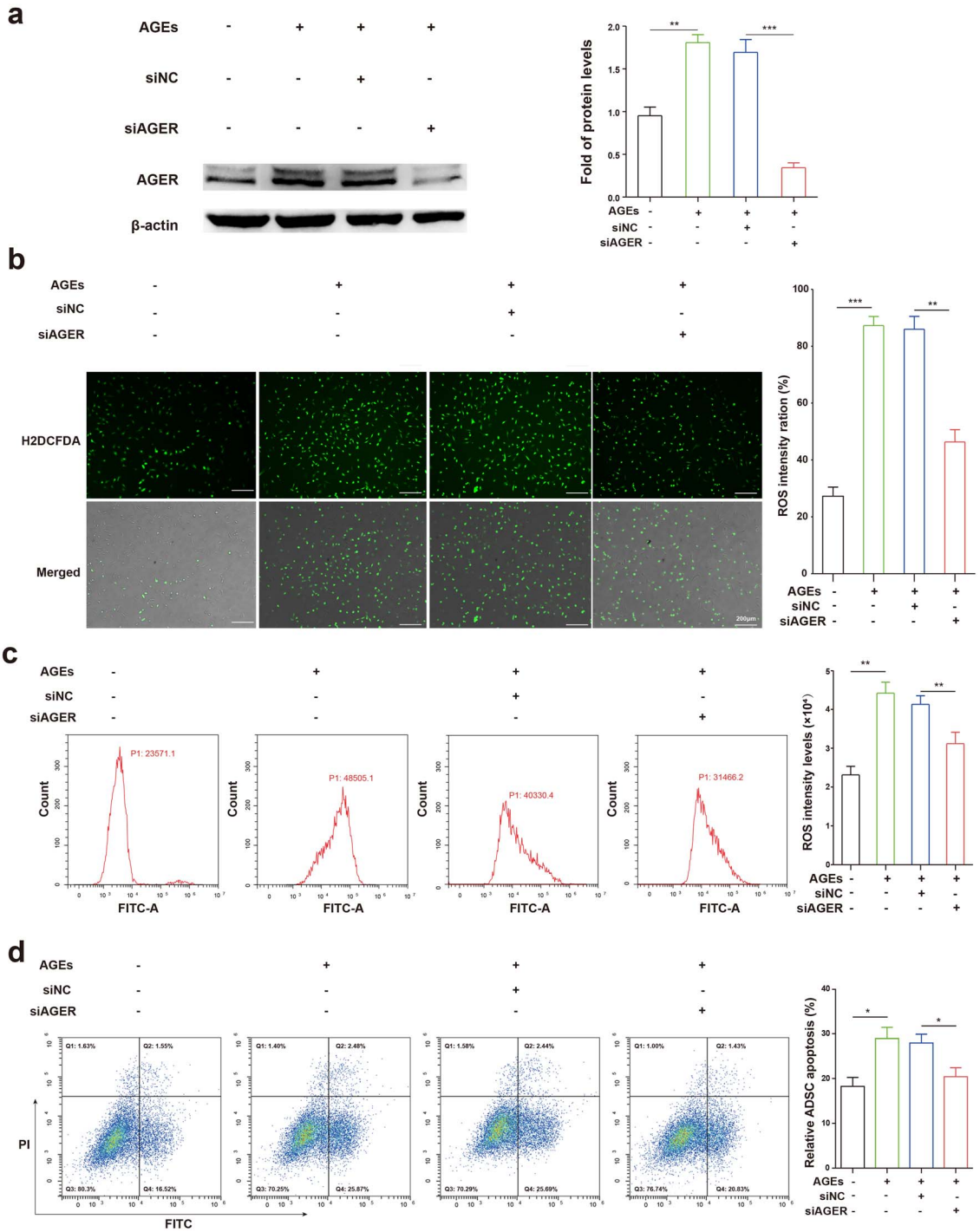

Figure 3. Effects of the AGE/AGER axis on ROS production and ADSC apoptosis. (**a**) Left: western blot shows AGER expression after transfection with siAGER; siRNA served as a negative control for siAGER. Right: quantitative analysis comparing AGER expression levels between the groups. (**b**) ROS production was tested by fluorescence microscope and the total cell number was observed by bright field microscopy to calculate the percentage. (**c**) Flow cytometry showing ROS levels in ADSCs. (**d**) FITC/PI stained ADSCs analyzed by flow cytometry. Data are shown as means ± SD. Statistical analysis: $^{*}p<0.05$, $^{**}p<0.01$ and $^{*}p<0.05$. *AGE* Advanced glycation end product, *AGER* AGE receptor, *ADSC* adipose-derived stem cell, *ROS* reactive oxygen species

PDTC exposure (Figure 4a). Moreover, Cur could inhibit AGEs-induced ROS production (Figure 4b, c). Cur and PDTC also could decrease ADSC apoptosis (Figure 4d). Therefore, it is possible that Cur suppresses NF-κB signaling, leading to ROS production and ADSC apoptosis.

Cur involved in the inhibitory effect of AGEs/AGER induced NF-κB transportation to the nucleus and caspase-3 activation in ADSCs

Since NF-κB signaling participated in ROS production and apoptosis, we evaluated whether Cur could regulate

Downloaded from academic.oup.com/burnstrauma/article/doi/10.1093/burnst/tkac001/6547993 by guest on 14 October 2026

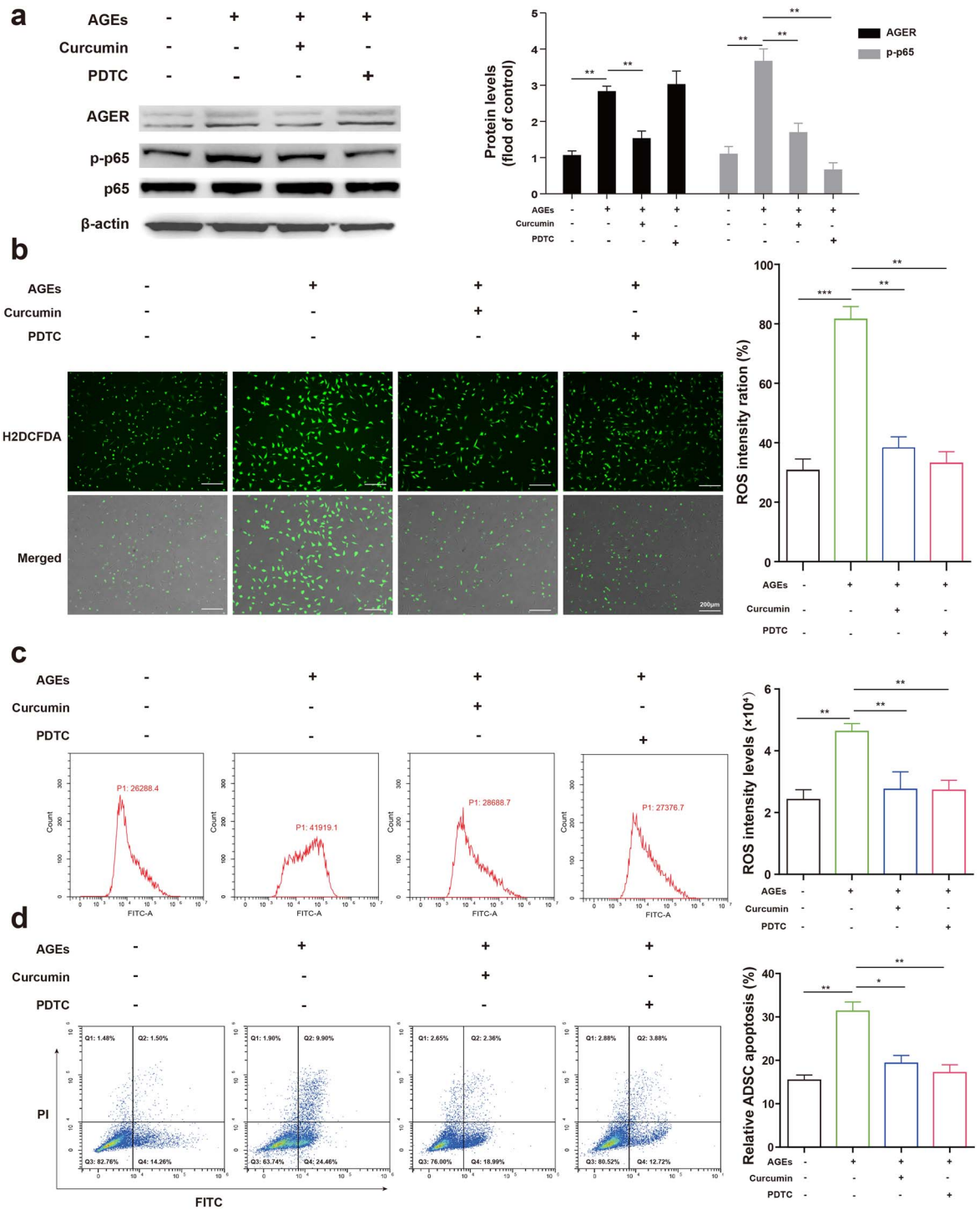

Figure 4. Cur suppresses AGEs/AGER axis-mediated ROS and ADSC apoptosis. (**a**) ADSCs pre-treated with AGEs were mixed with Cur or the p65 inhibitor PDTC (30 μM). Left: western blot demonstrates protein expression levels of AGER and phosphorylated and total p65. Right: comparison of AGER and p-p65 expression levels between the study groups. (**b**) ROS level was tested by fluorescence microscopy and total cell number was observed by bright field microscopy to calculate the percentage. (**c**) Flow cytometry showing ROS levels in ADSCs. (**d**) FITC/PI stained ADSCs analyzed by flow cytometry. Data are shown as means ± SD. Statistical analysis: $^{*}p<0.05$, $^{**}p<0.01$ and $^{*}p<0.001$. *AGE* Advanced glycation end product, *AGER* AGE receptor, *ROS* reactive oxygen species, *ADSC* adipose-derived stem cell, *Cur* curcumin, *PDTC* pyrrolidinedithiocarbamate

NF-κB p65. First, we detected AGER and p-p65 protein levels after Cur treatment for 0–24 h and incubation with AGEs (800 μg/mL) for 24 h. AGERs and p-p65 were down-regulated in response to Cur (Figure 5a). The transcription factor NF-κB p65 was involved in regulating gene transcription and apoptosis, which is normally activated during translocation from the cytoplasm to the nucleus. Translocation of p65 from the cytoplasm to the nucleus

Downloaded from academic.oup.com/burnstrauma/article/doi/10.1093/burnst/tkac001/6547993 by guest on 14 October 2026

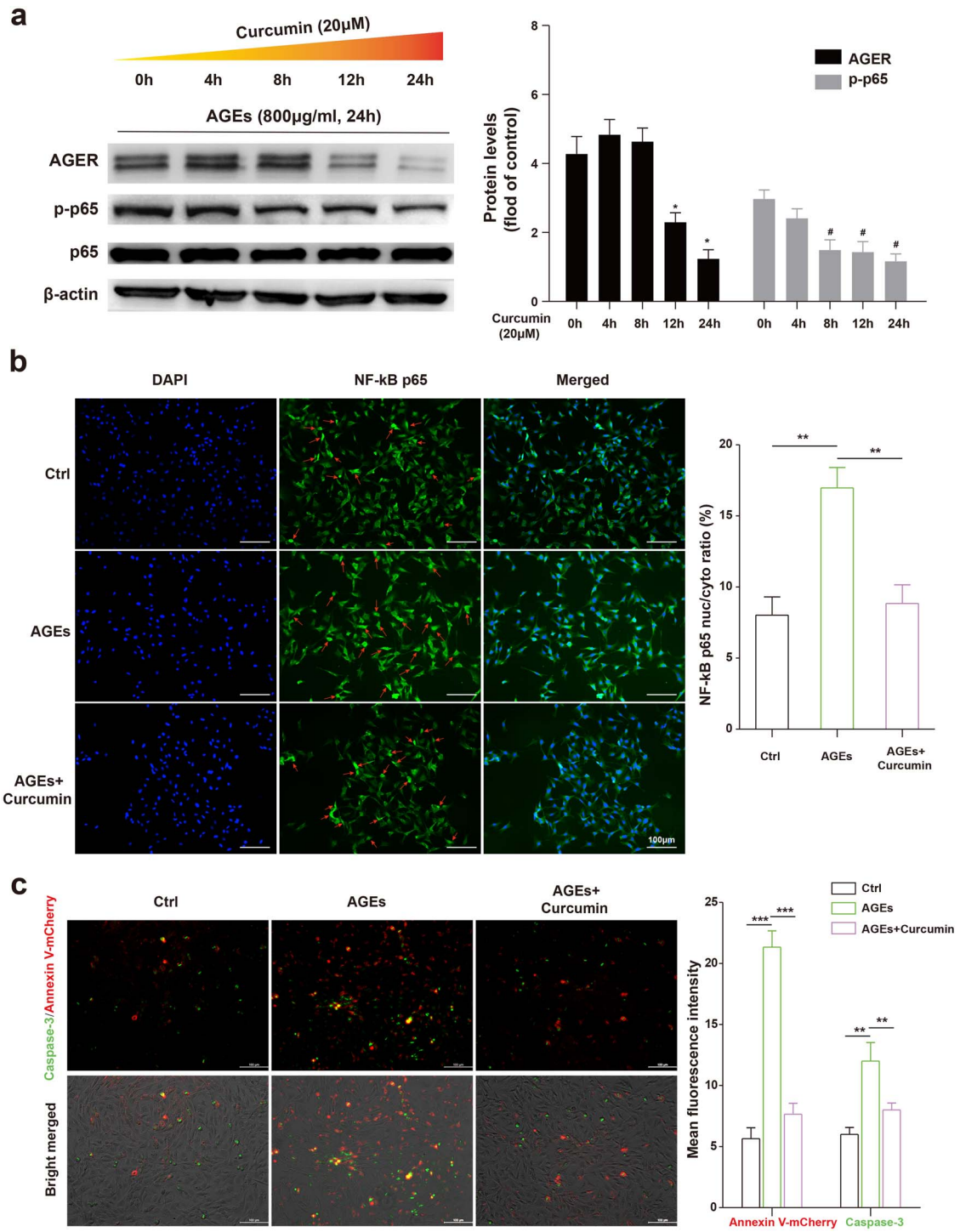

Figure 5. Role of NF-κB p65 signal in the inhibitory effect of Cur on ADSCs. (**a**) Left: time course analysis of AGER and phosphorylated and total p65 protein expression levels in ADSCs pre-treated with AGEs (800 μg/mL; 24 h) treated with Cur (20 μM). Right: comparison of AGER and p-p65 expression levels between the study groups. (**b**) ADSCs pre-treated with AGEs (800 μg/mL; 24 h) with or without Cur (20 μM; 24 h). Translocation of p65 from the cytoplasm to the nucleus was quantified by cell immunofluorescence staining (red arrowheads). (**c**) V-mCherry/caspase-3 stained ADSCs analyzed by flow cytometry. Relative fluorescence intensity was used to calculate cell apoptosis and caspase-3 expression level. Data are shown as means ± SD. Statistical analysis: $^{*}p<0.05$, $^{**}p<0.01$ and $^{*}p<0.001$. ($^{*}p$ *vs* 0 h of AGER, #*p vs* 0 h of p-p65). *NF-κB* nuclear factor-κB, *Cur* curcumin, *ADSC* adipose-derived stem cell, *AGE* advanced glycation end product, *AGER* AGE receptor

was detected using cell immunofluorescence staining. Cur significantly inhibited the translocation of p65 induced by AGEs (Figure 5b). Caspase-3, the principal apoptosis marker, is involved in the apoptosis induced by mitochondrial and cytosolic pathways [34]. Therefore, we evaluated caspase-3 activity using fluorescence microscopy and found that

Downloaded from academic.oup.com/burnstrauma/article/doi/10.1093/burnst/tkac001/6547993 by guest on 14 October 2026

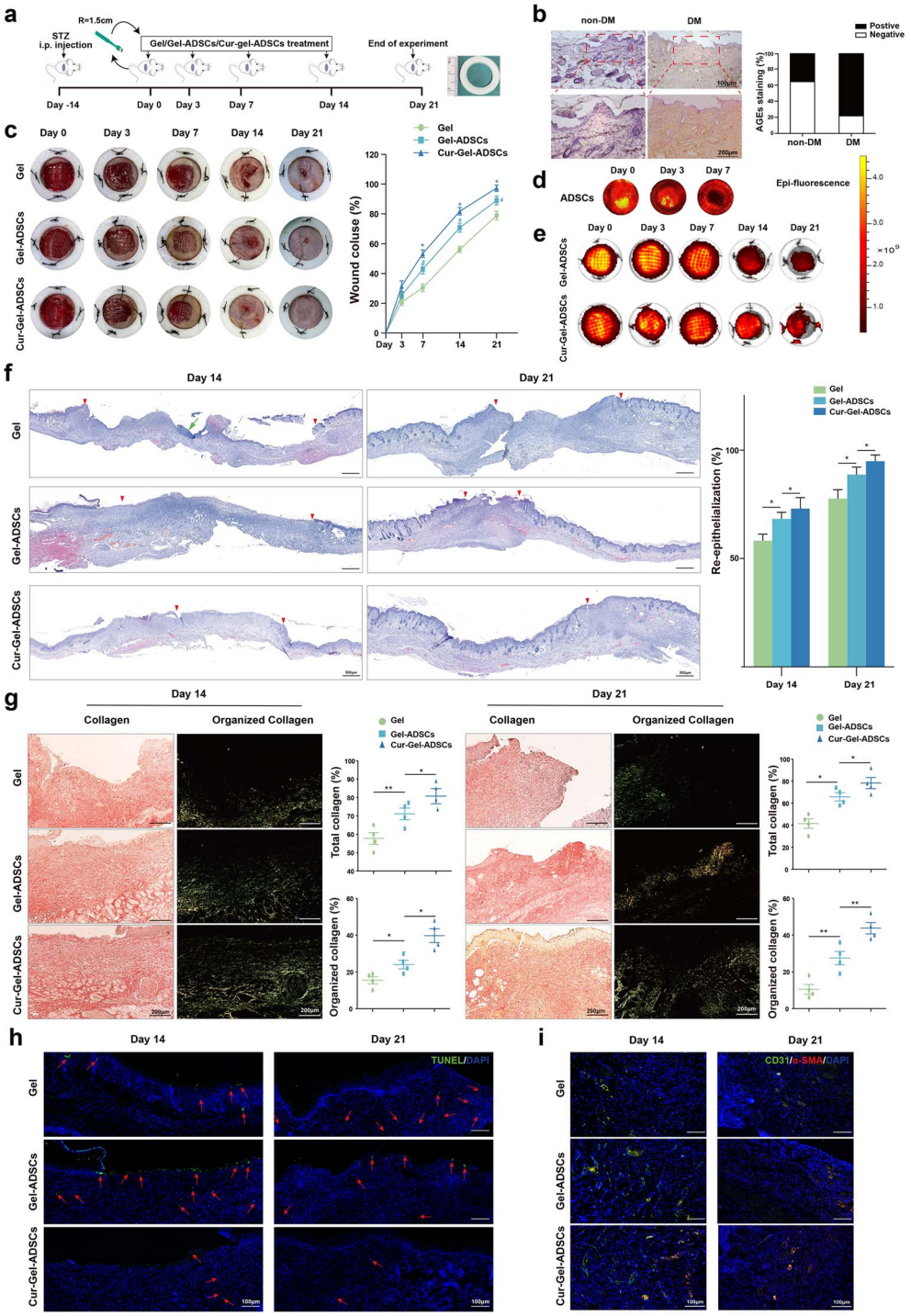

Figure 6. Cur-GelMA scaffold enhances ADSC survival and accelerates diabetic wound healing. (**a**) Above: schematic diagram of *in vivo* wound healing of nude mice. Below: schematic representation of 3D bioprinted GelMA scaffolds and *in vivo* transplantation. (**b**) Representative immunohistochemistry of AGEs in nude mice and streptozocin-induced nude mice skin tissue. Quantification of AGEs+ cells (%) analyzed using ImageJ software. (**c**) Left: gross appearance of the skin wounds after administration of GelMA, GelMA-ADSCs or Cur-GelMA-ADSCs. Excisional wound-splinting assay demonstrating improved wound closure with Cur-GelMA-ADSCs compared to the other scaffolds. Right: wound healing rate of each group. (**d**) IVIS was used to detect DiR fluorescence after DiR labelling of ADSCs transplanted on the surface of excisional wounds on days 0, 3 and 7. (**e**). IVIS was used to detect DiR fluorescence after DiR labelling of ADSCs in 3D printing scaffolds transplanted in excisional wounds on days 0, 3, 7, 14 and 21. The color scale is shown on the right side. (**f**) Left: representative H&E-stained sections on days 14 and 21 after wound creation. Pink arrows point to the epithelial tongues and green arrows to the GelMA of interest. Right: Percentage of re-epithelialization between the evaluated groups. (**g**) Left: representative SR-stained section on days 14 and 21 after wound creation. Right: the percentage of total collagen and organized collagen between the groups. (**h**) TUNEL fluorescence staining of wounds from the three groups on days 14 and 21 showed apoptosis (red arrowheads). **(i)** Representative immunofluorescence images on days 14 and 21 after wound creation showing the presence of $CD31^+$ and α-SMA^+ vessels. Data are shown as means ± SD. Statistical analysis: $^{**}p<0.05$, and $^{***}p<0.01$. ($^*p$ *vs* Gel-ADSCs, #*p vs* Gel.) *Gel-MA* gelatin methacryloyl, *ADSC* adipose-derived stem cell, *Cur* curcumin, *AGE* advanced glycation end product, *DiR* 1,1′-dioctadecyl-3,3,3′,3′-tetramethylindotricarbocyanine, *IVIS in vivo* imaging system, *H&E* hematoxylin and eosin, *SR* swelling ratio

Downloaded from academic.oup.com/burnstrauma/article/doi/10.1093/burnst/tkac001/6547993 by guest on 14 October 2026

the ADSC apoptosis induced by AGEs was significantly decreased by Cur through inhibition of the caspase-3 pathway (Figure 5c). Therefore, it is possible that Cur suppresses p65 signal activity, leading to ADSC apoptosis through the caspase-3 system.

Cur-GelMA scaffold promotes *in vivo* cell survival and diabetic wound healing

We applied a nude mouse model of full-thickness skin defect to verify that Cur-GelMA-ADSCs accelerate the diabetic cutaneous wound healing response. The animals were repeatedly treated with topical GelMA or Cur-GelMA scaffold obtained from a 3D bioprinter in the presence or absence of encapsulated DiR-ADSCs (Figure 6a). We injected DiR-marked ADSCs onto or into the chronic wounds. First, we used immunohistochemistry to detect AGE expression in the skin of normal and STZ-induced type 1 diabetic nude mice. AGE expression in diabetic nude mice was higher than that in normal nude mice (Figure 6b). Subsequently, treatment with GelMA-ADSCs significantly expedited re-epithelialization compared to treatment with GelMA. Importantly, topical application of Cur-GelMA-ADSC scaffold significantly accelerated wound healing compared to GelMA-ADSC treatment. H&E demonstrated a higher degree of wound re-epithelialization after 14 and 21 days in the Cur-GelMA-ADSC group compared to the GelMA and GelMA-ADSC groups (Figure 6c and f). In addition, we transplanted DiR-labeled ADSCs directly onto the surface of the wound and IVIS showed that only a small number of cells survived at day 7 (Figure 6d). DiR- labeled ADSCs were loaded into the GelMA and mice were administered topical GelMA-ADSCs with or without Cur. When the cells were loaded into Cur-GelMA, a greater number of living cells were detected on day 21 compared to GelMA-ADSCs (Figure 6e). Cur-GelMA-ADSCs increased the quantities of total and organized collagen (Figure 6g). We used a TUNEL assay to detect apoptosis in skin tissues. We found that Cur ameliorated apoptosis in skin tissue (Figure 6h). Furthermore, the detection of endothelial markers CD31 and α-SMA suggested that the blood vessels were mature, indicating that Cur-GelMA-ADSCs could induce angiogenesis (Figure 6i).

Discussion

ADSCs demonstrated strong differentiation and secretion abilities, increased the activity of vascular endothelial cells and keratinocytes and accelerated wound healing [35–37]. However, the persistence of hypoxia, inflammation and high glucose in the wound microenvironment leads to low survival rates after stem cell transplantation, limiting the efficacy of their cell therapy. In the present study, we demonstrated that ADSCs encapsulated in 3D printed GelMA had a greater proportion of living cells even 21 days after transplantation. The 3D-printed, grid-like scaffold increased the survival of the transplanted cells by facilitating the absorption of nutrients from the wound. Additionally, the 3D-printed grid-like scaffold was beneficial to the growth of new granulation and new blood vessels.

AGEs are toxic metabolic products produced by and accumulated in the diabetic microenvironment. AGEs stimulate the pathophysiological cascades related to diabetic complications. AGEs and AGERs comprise an important complex involved in cell dysfunction by increasing ROS production and decreasing ATP production and mitochondrial activity [13, 38]. Excessive AGEs accumulation, followed by AGER activation, is linked to aging and diabetic complications [39]. Apoptosis is one of the potential mechanisms by which AGEs affect cell function [40]. Excessive ROS production and AGEs induce apoptosis and impair diabetic wound healing. We found that AGEs upregulate AGER expression and cell apoptosis, which may be related to increased caspase-3 activity and sustained by NF-κB p65 activation. Future experiments should decrease caspase-3 activity to detect the role of AGEs/AGERs/NF-κB p65/caspase-3 in ADSC apoptosis.

Cur, extracted from the rhizome of Zingiberaceae, has antioxidant, anti-inflammatory and anti-apoptotic activities [41, 42]. Studies have shown that Cur is involved in cellular ROS production and apoptosis in MSCs [43]. In addition, liposomal Cur has been demonstrated to enhance the activity of endothelial-differentiated-human periodontal ligament stem cells and dental pulp stem cells as an anti-inflammatory strategy [44, 45]. In addition, Cur pretreated ADSCs can accelerate the re-epithelialization and angiogenesis of acid inflicted burn wounds [46]. Here, we demonstrated that Cur reduced AGE-induced AGER and caspase-3 expression, ROS production, apoptosis and NF-κB p65 activation. Additionally, Cur enhanced the survival of transplanted GelMA-ADSCs scaffolds on diabetic wounds and accelerated wound healing.

Stem cells and bioengineering skin substitutes are widely used to treat large full-thickness skin defects and chronic wounds [47], but there are several limitations to their use, such as decreased vitality, apoptosis and death of cells after transplantation [48, 49]. Several skin repair and regeneration treatments are available, and the stem cell-based method for biomaterial loading is preferred owing to its bioactivity and biocompatibility [50, 51]. Gelatine contains an arginine, glycine and aspartate sequence, which promotes cell attachment and proliferation on the scaffold, and a matrix metalloproteinase sequence that promotes cell migration and remodeling [52–54]. Crosslinks can be established under ultraviolet radiation at room temperature and neutral pH. However, methacrylation does not affect the function of gelatine. Additionally, 10% GelMA interconnecting channels are beneficial for nutrition/oxygen perfusion and neovascularization [28, 29] and they have suitable mechanical properties for 3D printing. In this study, Cur incorporated with GelMA was selected as the 3D printing bioink and was loaded with ADSCs to repair full-thickness skin defects of diabetic nude

Downloaded from academic.oup.com/burnstrauma/article/doi/10.1093/burnst/tkac001/6547993 by guest on 14 October 2026

mice. Furthermore, the incubation of ADSCs with Cur significantly downregulated AGER and inhibited ROS production and ADSC apoptosis, which contributes to angiogenesis and the re-epithelialization of wounds.

Conclusions

Cur-GelMA hydrogel fabricated by the 3D printing technique had good biocompatibility and enhanced wound healing by ameliorating ADSC apoptosis. Cur promoted tissue repair by mitigating AGE/AGER/NF-κB p65-induced ROS generation and ADSC apoptosis. This composite can repair or regenerate the skin. Further studies are required to investigate this promising biomaterial and its clinical potential for wound healing.

Abbreviations

ADSC: Adipose-derived stem cells; AGE: Advanced glycation end product; AGER: Advanced glycation end product receptor; Cur: Curcumin; DiR: 1,1′-Dioctadecyl-3,3,3′,3′-tetramethylindotricarbocyanine; FBS: Fetal bovine serum; GelMA: Gelatin methacryloyl; H&E: Hematoxylin and eosin; IVIS: *In vivo* imaging system; MSC: Mesenchymal stem cells; NF- κB: Nuclear factor-κB; PI: Propidium iodide; PDTC: Pyrrolidinedithiocarbamate; ROS: Reactive oxygen species; SEM: Scanning electron microscope; α-SMA: α Smooth muscle actin; SR: Swelling ratio; STZ: Streptozocin. DMEM/F12: Dulbecco's modified Eagle's medium/F12; PBS: Phosphate buffered saline; BMSC: Bone mesenchymal stem cell; AM: Acetoxymethyl ester; BCA: Bicinchoninin acid; RIPA: Radio-immunoprecipitation assay; DAPI: 4,6-diamino-2-phenyl indole; TUNEL; TdT-mediated dUTP nick end labeling.

Availability of data and materials

Data supporting the results of this study can be obtained from the corresponding author upon reasonable request.

Authors' contributions

CM.H., XG.W. and SZ.X. designed the experiment. TT.W., M.Y. and W.Z. participated in animal experiment. SZ.X., MR.Y. and RH.J. performed the cell experiment and material properties. SZ.X. and TT.W. participated in the writing of the manuscript. All authors read and approved the final manuscript.

Conflict of interest

None declared.

Ethics approval and consent to participate

All patients sign informed consent. All animal experiments were conducted at the Animal Center of Zhejiang University and approved by Animal Care and Use Committee.

Funding

This work was supported by Grants from Zhejiang Provincial Basic Public Welfare Research Program (LGF19H150008) and the Natural Science Foundation of Zhejiang province (LGF20H150004).

References

1. Frykberg RG, Banks J. Challenges in the treatment of chronic wounds. *Adv Wound Care (New Rochelle)*. 2015;4:560–82.
2. Rathmann W, Giani G. Global prevalence of diabetes: estimates for the year 2000 and projections for 2030. *Diabetes Care*. 2004;27:2568–9 author reply 9.
3. Game F. Treatment strategies for neuroischaemic diabetic foot ulcers. *Lancet Diabetes Endocrinol*. 2018;6:159–60.
4. Eke G, Mangir N, Hasirci N, MacNeil S, Hasirci V. Development of a UV crosslinked biodegradable hydrogel containing adipose derived stem cells to promote vascularization for skin wounds and tissue engineering. *Biomaterials*. 2017;129:188–98.
5. Wu Y, Liang T, Hu Y, Jiang S, Luo Y, Liu C, *et al*. 3D bioprinting of integral ADSCs-NO hydrogel scaffolds to promote severe burn wound healing. *Regen Biomater*. 2021;8:rbab014.
6. Gadelkarim M, Abushouk AI, Ghanem E, Hamaad AM, Saad AM, Abdel-Daim MM. Adipose-derived stem cells: effectiveness and advances in delivery in diabetic wound healing. *Biomed Pharmacother*. 2018;107:625–33.
7. Lin S, Zhang Q, Li S, Zhang T, Wang L, Qin X, *et al*. Antioxidative and angiogenesis-promoting effects of tetrahedral framework nucleic acids in diabetic wound healing with activation of the Akt/Nrf2/HO-1 pathway. *ACS Appl Mater Interfaces*. 2020;12:11397–408.
8. Kang HJ, Kumar S, D'Elia A, Dash B, Nanda V, Hsia HC, *et al*. Self-assembled elastin-like polypeptide fusion protein coacervates as competitive inhibitors of advanced glycation end-products enhance diabetic wound healing. *J Control Release*. 2021;333:176–87.
9. Thomas MC. Advanced glycation end products. *Contrib Nephrol*. 2011;170:66–74.
10. Shaikh-Kader A, Houreld NN, Rajendran NK, Abrahamse H. The link between advanced glycation end products and apoptosis in delayed wound healing. *Cell Biochem Funct*. 2019;37:432–42.
11. Zhang H, Ge S, He K, Zhao X, Wu Y, Shao Y, *et al*. FoxO1 inhibits autophagosome-lysosome fusion leading to endothelial autophagic-apoptosis in diabetes. *Cardiovasc Res*. 2019;115:2008–20.
12. Senatus LM, Schmidt AM. The AGE-RAGE Axis: implications for age-associated arterial diseases. *Front Genet*. 2017;8:187. https://doi.org/10.3389/fgene.2017.00187.
13. Xue J, Ray R, Singer D, Böhme D, Burz DS, Rai V, *et al*. The receptor for advanced glycation end products (RAGE) specifically recognizes methylglyoxal-derived AGEs. *Biochemistry*. 2014;53:3327–35.
14. Hu R, Wang MQ, Ni SH, Wang M, Liu LY, You HY, *et al*. Salidroside ameliorates endothelial inflammation and oxidative stress by regulating the AMPK/NF-κB/NLRP3 signaling pathway in AGEs-induced HUVECs. *Eur J Pharmacol*. 2020;867:172797. https://doi.org/10.1016/j.ejphar.2019.172797.
15. Montezano AC, Touyz RM. Reactive oxygen species, vascular Noxs, and hypertension: focus on translational and clinical research. *Antioxid Redox Signal*. 2014;20:164–82.
16. Aggarwal BB, Sundaram C, Malani N, Ichikawa H. Curcumin: the Indian solid gold. *Adv Exp Med Biol*. 2007;595:1–75.
17. Qu J, Zhao X, Liang Y, Zhang T, Ma PX, Guo B. Antibacterial adhesive injectable hydrogels with rapid self-healing, extensibility and compressibility as wound dressing for joints skin wound healing. *Biomaterials*. 2018;183:185–99.

Downloaded from academic.oup.com/burnstrauma/article/doi/10.1093/burnst/tkac001/6547993 by guest on 14 October 2026

18. Gupta SC, Patchva S, Koh W, Aggarwal BB. Discovery of curcumin, a component of golden spice, and its miraculous biological activities. *Clin Exp Pharmacol Physiol*. 2012;39:283–99.
19. Zhou X, Luo Z, Baidya A, Kim HJ, Wang C, Jiang X, *et al*. Biodegradable beta-Cyclodextrin conjugated Gelatin Methacryloyl microneedle for delivery of water-insoluble drug. *Adv Healthc Mater*. 2020;9:e2000527. https://doi.org/10.1002/adhm.202000527.
20. Luo Z, Sun W, Fang J, Lee K, Li S, Gu Z, *et al*. Biodegradable Gelatin Methacryloyl microneedles for transdermal drug delivery. *Adv Healthc Mater*. 2019;8:e1801054.
21. Liu Y, Zhao X, Zhao C, Zhang H, Zhao Y. Responsive porous microcarriers with controllable oxygen delivery for wound healing. *Small*. 2019;15:e1901254.
22. Jin R, Cui Y, Chen H, Zhang Z, Weng T, Xia S, *et al*. Three-dimensional bioprinting of a full-thickness functional skin model using acellular dermal matrix and gelatin methacrylamide bioink. *Acta Biomater*. 2021;131:248–61.
23. Lu YQ, Lu Y, Li HJ, Cheng XB. Effect of advanced glycosylation end products (AGEs) on proliferation of human bone marrow mesenchymal stem cells (MSCs) in vitro. *In Vitro Cell Dev Biol Anim*. 2012;48:599–602.
24. Scharstuhl A, Mutsaers HA, Pennings SW, Szarek WA, Russel FG, Wagener FA. Curcumin-induced fibroblast apoptosis and in vitro wound contraction are regulated by antioxidants and heme oxygenase: implications for scar formation. *J Cell Mol Med*. 2009;13:712–25.
25. Pan W, Dai C, Li Y, Yin Y, Gong L, Machuki JO, *et al*. PRP-chitosan thermoresponsive hydrogel combined with black phosphorus nanosheets as injectable biomaterial for biotherapy and phototherapy treatment of rheumatoid arthritis. *Biomaterials*. 2020;239:119851. https://doi.org/10.1016/j.biomaterials.2020.119851.
26. Chen MY, Xiao ZK, Lei XP, Li JX, Yu XY, Zhang JY, *et al*. Preparation, characterization and in vitro-in vivo evaluation of bortezomib supermolecular aggregation nanovehicles. *J Nanobiotechnology*. 2020;18:57. https://doi.org/10.1186/s12951-020-00612-7.
27. Yan Y, Wu R, Bo Y, Zhang M, Chen Y, Wang X, *et al*. Induced pluripotent stem cells-derived microvesicles accelerate deep second-degree burn wound healing in mice through miR-16-5p-mediated promotion of keratinocytes migration. *Theranostics*. 2020;10:9970–83.
28. Zhou F, Hong Y, Liang R, Zhang X, Liao Y, Jiang D, *et al*. Rapid printing of bio-inspired 3D tissue constructs for skin regeneration. *Biomaterials*. 2020;258:120287. https://doi.org/10.1016/j.biomaterials.2020.120287.
29. Chen YC, Lin RZ, Qi H, Yang Y, Bae H, Melero-Martin JM, *et al*. Functional human vascular network generated in Photocrosslinkable Gelatin methacrylate hydrogels. *Adv Funct Mater*. 2012;22:2027–39.
30. Asgari N, Bagheri F, Eslaminejad MB, Ghanian MH, Sayahpour FA, Ghafari AM. Dual functional construct containing kartogenin releasing microtissues and curcumin for cartilage regeneration. *Stem Cell Res Ther*. 2020;11:289. https://doi.org/10.1186/s13287-020-01797-2.
31. Zhao X, Wu H, Guo B, Dong R, Qiu Y, Ma PX. Antibacterial anti-oxidant electroactive injectable hydrogel as self-healing wound dressing with hemostasis and adhesiveness for cutaneous wound healing. *Biomaterials*. 2017;122:34–47.
32. Ganugula R, Arora M, Jaisamut P, Wiwattanapatapee R, Jorgensen HG, Venkatpurwar VP, *et al*. Nano-curcumin safely prevents streptozotocin-induced inflammation and apoptosis in pancreatic beta cells for effective management of type 1 diabetes mellitus. *Br J Pharmacol*. 2017;174:2074–84.
33. Tzeng TF, Liou SS, Tzeng YC, Liu IM. Zerumbone, a phytochemical of subtropical ginger, protects against Hyperglycemia-induced retinal damage in experimental diabetic rats. *Nutrients*. 2016;8:449. https://doi.org/10.3390/nu8080449.
34. Dubey M, Nagarkoti S, Awasthi D, Singh AK, Chandra T, Kumaravelu J, *et al*. Nitric oxide-mediated apoptosis of neutrophils through caspase-8 and caspase-3-dependent mechanism. *Cell Death Dis*. 2016;7:e2348. https://doi.org/10.1038/cddis.2016.248.
35. Mazini L, Rochette L, Admou B, Amal S, Malka G. Hopes and limits of adipose-derived stem cells (ADSCs) and mesenchymal stem cells (MSCs) in wound healing. *Int J Mol Sci*. 2020;21:1306.
36. Luck J, Smith OJ, Malik D, Mosahebi A. Protocol for a systematic review of autologous fat grafting for wound healing. *Syst Rev*. 2018;7:99. https://doi.org/10.1186/s13643-018-0769-7.
37. Tseng YC, Roan JN, Ho YC, Lin CC, Yeh ML. An in vivo study on endothelialized vascular grafts produced by autologous biotubes and adipose stem cells (ADSCs). *J Mater Sci Mater Med*. 2017;28:166.
38. Lo MC, Chen MH, Lee WS, Lu CI, Chang CR, Kao SH, *et al*. Nε-(carboxymethyl) lysine-induced mitochondrial fission and mitophagy cause decreased insulin secretion from β-cells. *Am J Physiol Endocrinol Metab*. 2015;309:E829–39. https://doi.org/10.1152/ajpendo.00151.2015
39. Lubitz I, Ricny J, Atrakchi-Baranes D, Shemesh C, Kravitz E, Liraz-Zaltsman S, *et al*. High dietary advanced glycation end products are associated with poorer spatial learning and accelerated Abeta deposition in an Alzheimer mouse model. *Aging Cell*. 2016;15:309–16.
40. Maeda S, Matsui T, Takeuchi M, Yamagishi S. Sodium-glucose cotransporter 2-mediated oxidative stress augments advanced glycation end products-induced tubular cell apoptosis. *Diabetes Metab Res Rev*. 2013;29:406–12.
41. Li W, Suwanwela NC, Patumraj S. Curcumin by down-regulating NF-kB and elevating Nrf2, reduces brain edema and neurological dysfunction after cerebral I/R. *Microvasc Res*. 2016;106:117–27.
42. Tu ZL, Lin C. Research advances on the effects and mechanism of curcumin in promoting diabetic wound healing. *Chinese journal of burns*. 2021;37:391–4.
43. Yagi H, Tan J, Tuan RS. Polyphenols suppress hydrogen peroxide-induced oxidative stress in human bone-marrow derived mesenchymal stem cells. *J Cell Biochem*. 2013;114:1163–73.
44. Sinjari B, Pizzicannella J, D'Aurora M, Zappacosta R, Gatta V, Fontana A, *et al*. Curcumin/liposome nanotechnology as delivery platform for anti-inflammatory activities via NFkB/ERK/pERK pathway in human dental pulp treated with 2-HydroxyEthyl MethAcrylate (HEMA). *Front Physiol*. 2019;10:633.
45. Diomede F, Fonticoli L, Guarnieri S, Della Rocca Y, Rajan TS, Fontana A, *et al*. The effect of liposomal curcumin as an anti-inflammatory strategy on lipopolysaccharide e from Porphyromonas gingivalis treated endothelial committed neural crest derived stem cells: morphological

Downloaded from academic.oup.com/burnstrauma/article/doi/10.1093/burnst/tkac001/6547993 by guest on 14 October 2026

and molecular mechanisms. *Int J Mol Sci*. 2021;22:7534. https://doi.org/10.3390/ijms22147534.

46. Azam M, Ghufran H, Butt H, Mehmood A, Ashfaq R, Ilyas AM, *et al*. Curcumin preconditioning enhances the efficacy of adipose-derived mesenchymal stem cells to accelerate healing of burn wounds. *Burns Trauma*. 2021;9:tkab021. https://doi.org/10.1093/burnst/tkab021.
47. Guo R, Ward CL, Davidson JM, Duvall CL, Wenke JC, Guelcher SA. A transient cell-shielding method for viable MSC delivery within hydrophobic scaffolds polymerized in situ. *Biomaterials*. 2015;54:21–33.
48. Li S, Stöckl S, Lukas C, Götz J, Herrmann M, Federlin M, *et al*. hBMSC-derived extracellular vesicles attenuate IL-1β-induced catabolic effects on OA-chondrocytes by regulating pro-inflammatory Signaling pathways. *Front Bioeng Biotechnol*. 2020;8:603598. https://doi.org/10.3389/fbioe.2020.603598.
49. Wang X, Shen K, Wang J, Liu K, Wu G, Li Y, *et al*. Hypoxic preconditioning combined with curcumin promotes cell survival and mitochondrial quality of bone marrow mesenchymal stem cells, and accelerates cutaneous wound healing via PGC-1α/SIRT3/HIF-1α signaling. *Free Radic Biol Med*. 2020;159:164–76.
50. Bhardwaj N, Chouhan D, Mandal BB. Tissue engineered skin and wound healing: current strategies and future directions. *Curr Pharm Des*. 2017;23:3455–82.
51. Mao AS, Mooney DJ. Regenerative medicine: current therapies and future directions. *Proc Natl Acad Sci U S A*. 2015;112:14452–9.
52. Liu Y, Chan-Park MB. A biomimetic hydrogel based on methacrylated dextran-graft-lysine and gelatin for 3D smooth muscle cell culture. *Biomaterials*. 2010;31:1158–70.
53. Ma L, Gao C, Mao Z, Zhou J, Shen J, Hu X, *et al*. Collagen/chitosan porous scaffolds with improved biostability for skin tissue engineering. *Biomaterials*. 2003;24:4833–41.
54. Ma T, Fu B, Yang X, Xiao Y, Pan M. Adipose mesenchymal stem cell-derived exosomes promote cell proliferation, migration, and inhibit cell apoptosis via Wnt/β-catenin signaling in cutaneous wound healing. *J Cell Biochem*. 2019;120:10847–54.

Downloaded from academic.oup.com/burnstrauma/article/doi/10.1093/burnst/tkac001/6547993 by guest on 14 October 2026